Phase Behavior of Polystyrene−Poly(2-vinylpyridine) Diblock Copolymers

Mark F. Schulz,† Ashish K. Khandpur,† and Frank S. Bates*

Department of Chemical Engineering and Materials Science, University of Minnesota, Minneapolis, Minnesota 55455

Kristoffer Almdal and Kell Mortensen

Risø National Laboratory, DK-4000 Roskilde, Denmark

Damian A. Hajduk‡ and Sol M. Gruner

Department of Physics, Princeton University, Princeton, New Jersey 08544-0708

Received November 17, 1995; Revised Manuscript Received February 5, 1996[⊗]

ABSTRACT: We characterize the phase behavior of a series of polystyrene−poly(2-vinylpyridine) diblock copolymers ($M_w \sim 20\,000$ g/mol) using dynamic mechanical spectroscopy, transmission electron microscopy, small-angle neutron scattering, and small-angle X-ray scattering. Measurements on symmetric diblocks ($f_{PS} = 0.5$) permit us to estimate the Flory−Huggins interaction parameter (χ) for this system, which we use to place our findings on a diagram. Four ordered morphologies (lamellae, hexagonally perforated layers, bicontinuous cubic/gyroid, and hexagonally packed cylinders) are found at compositions ranging from 35 to 70 vol % polystyrene. An order−order transition separates the hexagonally perforated layer and $Ia\bar{3}d$/gyroid phases at 38 vol % styrene. Studies of shear-oriented material indicate that the cubic microstructure does not appear to grow with a preferred orientation from the layered phase, in contrast to recent findings in other diblock systems. The occurrence of complex phases at compositions between those at which lamellar and cylindrical phases are observed appears to be a general feature of low molecular weight diblock copolymer melts.

Introduction

The morphology formed by a microphase-separated block copolymer melt is thought to depend primarily on the number of statistical segments (N), the degree of immiscibility between the two monomer types (χ, the Flory−Huggins interaction parameter), and the volume fraction occupied by the minority component in the molecule (f). The segregation product χN is the principal determinant of the degree to which the melt is microphase-separated, while the minority component volume fraction determines the particular morphology observed when the melt undergoes microphase separation. More recent work[1−4] suggests that a fourth parameter, a conformational asymmetry parameter (ϵ) which describes differences in the way that the two blocks fill their respective domains, also influences phase behavior.

Initial attempts at mapping this phase behavior were performed in the strong segregration limit (SSL), where $\chi N \rightarrow \infty$. In this limit, the phase boundaries separating ordered morphologies become nearly independent of segregation, and so different microphases were accessed by changing the composition (f) of the system. Polyisoprene−polystyrene (PI−PS) diblock copolymers, the most extensively studied system,[5−8] were reported to exhibit the following morphologies in the SSL:[1] spheres arranged on a BCC ($Im\bar{3}m$ space group) lattice for $f_{PI} > 0.78$ or < 0.18, hexagonally packed cylinders (HEX) for $0.78 > f_{PI} > 0.68$ and $0.31 > f_{PI} > 0.18$, lamellae (LAM) for $0.60 > f_{PI} > 0.31$, and a bicontinuous double-diamond structure (OBDD) ($Pn\bar{3}m$ space group) for $0.68 > f_{PI} > 0.60$. The last stucture was first reported for starblock copolymers;[9] a recent reevaluation of some of these starblock materials has revealed that the bicontinuous cubic microstructure present actually belongs to the $Ia\bar{3}d$ space group.[10] Although the presence of the BCC (spheres), HEX, and LAM phases and the value of the composition f_{PI} for their corresponding phase transitions are in good agreement with theoretical calculations in the SSL,[11,12] the occurrence of the OBDD phase has not been predicted in block copolymer melts.[13−17]

More recent work has exploited the temperature dependence of χ to cross phase boundaries and produce transitions between different ordered microphases.[18−27] Such studies are performed in the weak segregation limit (WSL) ($\chi N \lesssim 10$), where the phase boundaries acquire significant curvature in the $\chi N - f$ plane. The WSL encompasses the various ordered phases and the disordered phase near the order−disorder transition (ODT).[28] Experiments on a variety of model hydrocarbon systems near the ODT[2,18−21,26,27] have demonstrated a richer phase behavior between the LAM and HEX states than predicted theoretically.[15,29−31] Such studies have led to the discovery of hexagonally modulated lamellae (HML),[2,19,20] hexagonally perforated layers (HPL),[2,19−21,26,27] and a bicontinuous phase with $Ia\bar{3}d$ space group symmetry;[2,21−23,26,27] the latter is often referred to as the gyroid* (G) phase. Theoretical calculations have predicted the G/$Ia\bar{3}d$ phase,[15] but not the HML or HPL phase,[15,32] to be stable in diblock copolymer melts.

Several factors have been considered in an attempt to explain the complex phase behavior observed in the WSL. Theoretical[30−35] and experimental[2,36−38] work suggests that phase behavior in this limit is strongly influenced by composition fluctuations arising from the finite lengths of the copolymer chains; as the chains

* To whom correspondence should be addressed.
† Current address: 3M Co., 3M Center, St. Paul, MN 55144.
‡ Current address: Department of Chemical Engineering and Materials Science, University of Minnesota, Minneapolis, MN 55455.
[⊗] Abstract published in *Advance ACS Abstracts,* March 15, 1996.

0024-9297/96/2229-2857$12.00/0

become infinitely long, mean-field-like behavior is restored. At a constant degree of segregation, then, a diblock copolymer with a small χ and large N (*e.g.*, polyethylene−poly(ethylene-*co*-propylene), where $\chi \sim 0.012$ at 120 °C[39]) will display nearly mean-field behavior, while a material with a large χ and small N (*e.g.*, polyisoprene−polystyrene, where $\chi \sim 0.05$ at 120 °C[40]) will be more influenced by fluctuation effects. We have summarized the effects of finite molecular weights in several hydrocarbon diblock copolymer systems in a separate report.[2] The results indicate that lower molecular weight diblock systems exhibit the G/*Ia*$\bar{3}$*d* bicontinuous phase near the ODT, whereas high molecular weight systems do not.

In this work, we investigate the universality of this conclusion. The polystyrene−poly(2-vinylpyridine) (PS−PVP) system is well suited for the study of finite molecular weight effects. Due to the relatively large incompatibility between these monomer types ($\chi \sim 0.1$), microphase separation can be observed in PS−PVP materials of relatively low molecular weights (∼20 000 g/mol). To the best of our knowledge, the phase behavior of PS−PVP diblock copolymer melts near the ODT has not been previously reported. Using a combination of dynamic mechanical spectroscopy (DMS), transmission electron microscopy (TEM), and small-angle neutron and X-ray scattering (SANS and SAXS), we identify the microstructures formed in a series of PS−PVP diblocks with overall PS volume fractions from 0.35 to 0.70. Also, the temperature dependence of χ is estimated using the ODT temperatures from a series of symmetric PS−PVP diblocks. Using this expression, the diblock results are presented on a single phase diagram.

Experimental Section

Materials. Styrene monomer (both normal (Aldrich) and perdeuterated (Aldrich, 98+ atom % D)) was purified by successive vacuum distillations from CaH_2 (Aldrich) and dibutylmagnesium (Aldrich). The 2-vinylpyridine monomer (Aldrich) was likewise purified from CaH_2 and triethylaluminum (Aldrich). Tetrahydrofuran (THF) (Fisher) was purified by distillation from fresh sodium with benzophenone (Aldrich) for the anionic polymerizations. *sec*-Butyllithium in cyclohexane (Aldrich) was used as received, after titrating for active initiator concentration (*ca.* 1.3 M) using the Gilman method.[41] Methanol (EM Science) was deoxygenated by successive freezing, vacuum pumping, and thawing. Hexanes (EM Science) were used as received.

Synthesis. PS−PVP diblock copolymers were synthesized by the sequential anionic polymerization method, conducted under purified argon in a Pyrex reactor fitted with Viton O-ring-sealed joints and Teflon or Viton O-ring-sealed valves. Each monomer was distilled into a Pyrex burette fitted with Teflon valves and attached to the reactor. THF was distilled directly into the reactor and cooled to −78 °C. An aliquot of *sec*-butyllithium (initiator) was added to the well-stirred solvent through a septum using a gas-tight syringe. Next, the styrene was added dropwise; the rate of monomer addition was regulated so that the reactor temperature remained below −70 °C. Fifteen minutes after the styrene addition was complete, a second block was created by slowly adding the 2-vinylpyridine, again maintaining similar reactor temperature conditions. Polymerization of both monomers under these conditions is very rapid, and essentially complete conversion is obtained within several minutes. After waiting another 15 min, the reaction was terminated by injecting several milliliters of degassed methanol. The PS−PVP product was isolated from solution (*ca.* 5%, w/v) by precipitation in hexanes and vacuum-dried. Nearly complete conversions (>99%) were realized, allowing the block composition to be specified with about 1% precision.

Molecular Characterization. Gel permeation chromatography (GPC) traces were obtained from an instrument fitted with Phenogel (Phenomenex) columns and operated at room temperature with THF as the mobile phase at a flow rate of 1 mL/min. Elution times were monitored with a differential refractometer following injection of 100 μL of 0.1% (w/v) polymer solutions. The instrument was calibrated with a series of monodisperse polystyrene standards (Pressure Chemical Co.). GPC results verified the block copolymer molecular weights calculated from the monomer/initiator ratio, and in all cases we determined a polydispersity index $M_w/M_n \lesssim 1.06$. Polystyrene volume fractions, f_{PS}, were calculated from the synthesis stoichiometry, assuming densities of 1.01×10^{-2} mol/cm^3 for PS and 1.09×10^{-2} mol/cm^3 for PVP.

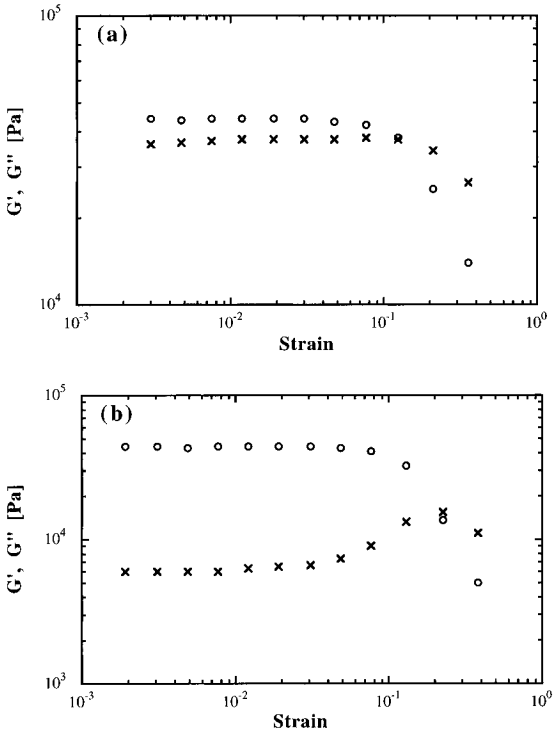

Figure 1. Effect of strain amplitude on the dynamic elastic (G', ○) and loss (G'', ×) shear moduli using a frequency of $\omega = 0.5$ rad/s: (a) $f_{PS} = 0.38$ at 140 °C (shown later to be the HPL morphology) and (b) $f_{PS} = 0.38$ at 160 °C (shown later to be the bicontinuous *Ia*3*d*/gyroid (G/*Ia*3*d*) morphology). The dynamic moduli become significantly nonlinear above about 6% strain for both phases.

Rheological Measurements. Phase transitions in block copolymer melts are generally accompanied by measurable changes in mechanical properties such as the dynamic elastic shear and loss moduli (G' and G'', respectively). Rheological measurements of these quantities have proven useful in determining order−order[18,19,21] and order−disorder[39] transition temperatures. Furthermore, isothermal frequency scans have been shown to provide a characteristic signature for different morphologies. This can provide a preliminary microstructural assignment which must then be confirmed by other techniques.

In this work, most dynamic mechanical shear measurements were performed with a Rheometrics solids analyzer (RSA II) operated with a 0.5 mm gap shear sandwich fixture, using 2−5% strain amplitude and frequencies ranging from 100 to 0.01 rad/s. Identification of the linear viscoelastic regime for certain samples employed a frequency of 0.5 rad/s and strain amplitudes from 0.2% to 30%. Since the molecular weights of each block are smaller than the critical molecular weights for entanglement coupling ($M_e = 13\,300$ kg/mol for PS and 28 600 kg/mol for PVP), the rheometer could be operated at frequencies well below the inverse terminal relaxation time of individual chains. In this limit, the mechanical response of the polymers is sensitive to the microstructure of the system. The viscoelastic response of the materials does not deviate significantly from linearity for $\gamma < 0.06$ (Figure 1); thus, the shear amplitude employed represented a compromise between having sufficient mechanical response to produce measurable stresses while remaining near

the linear viscoelastic regime. Temperature was controlled to within 1 °C by a nitrogen-filled gas convection oven. All measurements were taken above 140 °C to avoid the portion of the relaxation spectrum associated with the glass transition (T_g, the glass transition temperature, is *ca.* 100 °C for PS and PVP).

Isochronal (constant frequency) temperature scans were conducted at heating rates of about 1 °C/min to monitor for sudden changes in G' associated with order−order transitions. Isochronal traces for all materials were characterized by an elastic modulus (G') that dropped precipitously at a certain temperature. Frequency sweeps above this temperature showed the expected terminal behavior $G' \sim \omega^2$ and $G'' \sim \omega$, where ω is the deformation frequency; a sudden drop in G' was therefore interpreted as signifying the ODT.

Transmisson Electron Microscopy. Unsheared samples for electron microscopy were prepared by annealing the sample above the rheologically determined ODT temperature for 30 min followed by quenching in liquid nitrogen and subsequent annealing for at least 6 h at the temperature of interest. Subsequent quenching in liquid nitrogen froze in the low-temperature morphology. Sections of *ca.* 70 nm thickness were cut from the bulk specimen using a Reichert Ultracut S microtome. Microtomy was conducted at room temperature using glass or diamond knives. Sections were picked up on 400-mesh uncoated copper grids and then stained in the vapor of I_2 crystals. This treatment selectively stains the PVP domains,[42] which appear dark in the micrographs presented here. TEM was performed on a Jeol 100CX electron microscope operated at 100 kV. In order to facilitate analysis of the low-temperature phase of the $f_{PS} = 0.38$ specimen, samples of this polymer were shear-aligned during low-temperature annealing as described below prior to quenching in liquid nitrogen.

Small-Angle Neutron Scattering. Experiments were conducted on the NIST/Exxon/University of Minnesota 30m instrument at the National Institute of Standards and Technology (NIST) in Gaithersburg, MD, and on the 12m instrument at Risø National Laboratory, Roskilde, Denmark. At NIST, $\lambda = 5.5$ Å wavelength neutrons ($\Delta\lambda/\lambda = 0.14$) were used with a sample-to-detector distance of 3.4 m; the corresponding values for Risø were $\lambda = 5.54$ Å, $\Delta\lambda/\lambda = 0.09$, and a sample-to-detector distance of 3.0 m. Pinhole collimation and area detectors were employed at both facilities; data are reported below in arbitrary units of intensity.

The initial microstructure of specimens for SANS analysis were shear-aligned to facilitate structural analysis. Oriented samples were prepared either by "preshearing" the material before placement on the beam line or by use of an *in situ* shearing device as described elsewhere.[38,43] "Presheared" specimens were prepared using several hours of oscillatory shearing ($\gamma = 1$, $\dot{\gamma} \cong 0.13$ s^{-1}) between 5 × 5 cm Teflon-coated plates in a nitrogen environment at 140 °C as described elsewhere.[18,36,38,44] After shearing, samples were quiescently annealed at 140 °C for about 20 min before cooling below the glass transition temperatures of PS and PVP in order to freeze in the initial microstructure. Samples measuring 2 × 2 × 1 mm (approximately) were cut and mounted in specific orientations onto quartz windows prior to placement in the neutron beam. Due to the low molecular weights of the polymers, both blocks were unentangled, and the shear-oriented films were extremely brittle in the glassy state. The small size of the quenched specimens represents a compromise between keeping track of the shear geometry and minimizing multiple scattering from the specimen. Scattering was recorded from all of the presheared specimens with the neutron beam along the *x* (shear), *y* (shear gradient), and *z* (neutral) axes; the experimental geometry appears in Figure 2.

In situ experiments were performed in a helium atmosphere in order to reduce polymer degradation at high temperatures and minimize attenuation of the neutron beam. Sample thicknesses of 0.2, 0.4, or 1.0 mm and strain amplitudes of 100%, 300%, or 500% were used. SANS experiments can only be performed with the neutron beam directed normal to the plane of shear while the *in situ* device is operated. However, the polymer can be rapidly quenched below T_g by immersion in liquid nitrogen and then examined with an arbitrary neutron beam orientation using the same sample recovery and mounting procedure described in the preceding paragraph.

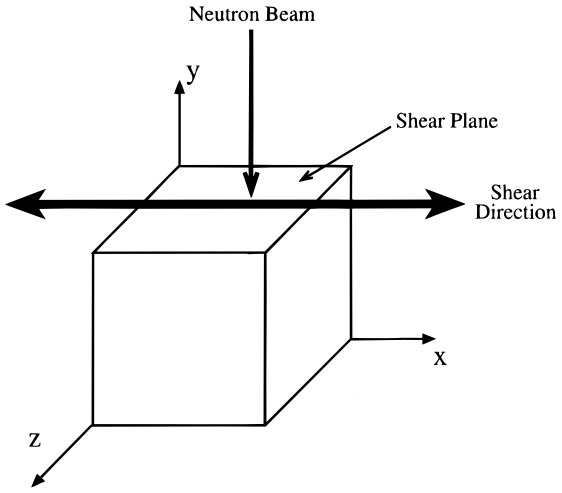

Figure 2. Coordinate system for SANS experiments. Neutron beam direction indicated relates to the combined (*in situ*) dynamic shear and SANS experiments while the shear field is being applied. Materials sheared with this instrument as well as presheared materials can be quenched below the glass transition temperature to freeze the morphology and subsequently examined with arbitrary neutron beam orientation (usually along *x*, *y*, and *z* directions).

Difficulties in aligning one of the sample axes with the neutron beam occasionally produced "asymmetric" images, in which stronger reflections were observed on one side of the neutron beam, or "rotated" ones, in which the observed reflections were rotated about the beam axis. These minor misalignments did not significantly affect the relative peak positions. The data are presented as contour plots where contour levels depict variations in intensity in decade increments; data surrounding the circular beam stop have been masked out. Unless otherwise noted, data from different scattering directions cannot be compared due to variations in path length through the sample; contour levels are not necessarily shown on the same scale. Contour plot axes are shown in units of $q = |\mathbf{q}| = 4\pi\lambda^{-1}\sin(\theta/2)$, where θ is the scattering angle and λ is the wavelength of the neutrons.

Small-Angle X-ray Scattering. SAXS measurements were performed using Cu Kα X-rays generated by a Rigaku RU-200BH rotating anode X-ray generator equipped with a 0.2 × 2 mm microfocus cathode and Franks mirror optics. Samples were placed inside an evacuated sample chamber and maintained at a constant temperature by a set of thermoelectric devices. Two-dimensional diffraction images were collected with an image-intensified area detector designed around a Thomson CCD chip.[45] After collection, the images were digitized and corrected for detector response characteristics. Intensities were then integrated azimuthally within a 30° angle about the film normal axis to obtain a one-dimensional radial plot.

Results

Table 1 lists the polystyrene volume fraction (f_{PS}) and the degree of polymerization for each of the 11 diblock copolymers employed in the present study. Five of the polymers are compositionally symmetric ($f_{PS} = 0.50$), while the remaining six are compositionally asymmetric. The phase behavior of each material has been characterized using rheological measurements; all of the asymmetric polymers, and one of the symmetric ones, were also characterized by TEM and small-angle scattering. Since these experimental techniques have been shown to be effective in establishing block copolymer phase behavior in several other systems,[19−22,27,43,46] only a few representative examples are discussed in detail.

Table 1. Molecular Characteristics of PS−PVP Diblock Copolymers

sample code	f_{PS}[b]	N_n	phase transitions[c,d]
SV-10[a]	0.34_8	203	HEX $\xrightarrow{207}$ DIS
SV-8[a]	0.37_5	192	HPL $\xrightarrow{146}$ $Ia\bar{3}d$ $\xrightarrow{180}$ DIS
SV-12[a]	0.39_9	209	LAM $\xrightarrow{232}$ DIS
SV-20	0.49_7	143	LAM $\xrightarrow{180}$ DIS
SV-18	0.50_0	200	LAM $\xrightarrow{250}$ DIS
SV-19	0.50_3	229	LAM $\xrightarrow{297}$ DIS
SV-17	0.50_4	171	LAM $\xrightarrow{212}$ DIS
SV-15[a]	0.50_5	157	LAM $\xrightarrow{185}$ DIS
SV-13[a]	0.63_2	208	LAM $\xrightarrow{233}$ DIS
SV-9[a]	0.65_2	196	HPL $\xrightarrow{175}$ DIS
SV-14[a]	0.70_3	209	HEX $\xrightarrow{210}$ DIS

[a] Synthesized using perdeuterated styrene. [b] PS volume fraction in the diblock copolymer, f_{PS}, is based on PS and PVP densities of 1.01×10^{-2} mol/cm^3 and 1.09×10^{-2} mol/cm^3, respectively. [c] Numbers above arrows indicate the approximate phase transition temperature in °C as determined from dynamic mechanical measurements. [d] Phase allocations: lamellae (LAM), hexagonally perforated layers (HPL), bicontinuous microstructure with $Ia\bar{3}d$ space group symmetry (G/$Ia\bar{3}d$), hexagonally packed cylinders (HEX), disordered (DIS).

Samples with f_{PS} between 0.40 and 0.63 displayed a single phase at low temperatures; isochronal temperature scans measured in the $f_{PS} = 0.50$ materials appear in Figure 3a. Isothermal frequency scans of these materials (Figure 3b) show a low overall elasticity characteristic of a discontinuous structure. TEM from unsheared specimens (Figure 3c) show the alternating light and dark bands with sharp light−dark interfaces that characterize the lamellar morphology. SANS from presheared specimens (Figure 3d) reveal an oriented morphology in which peaks appear in the $\mathbf{q}_x-\mathbf{q}_y$ and $\mathbf{q}_y-\mathbf{q}_z$ planes at spacings of q^* and $2q^*$; images of the $\mathbf{q}_x-\mathbf{q}_z$ (shear) plane display a powder-like ring with only a slight azimuthal variation in scattered intensity. This scenario is indicative of a well-oriented lamellar phase in which most (but not all) of the lamellar normals are parallel to the shear gradient direction, consistent with the TEM results.

Rheological results for the five samples with $f_{PS} = 0.50$ indicate that T_{ODT} increases with increasing molecular weight; see Table 1 and Figure 3a. Since microphase-separated symmetric diblocks are always characterized by a lamellar phase, faster heating rates of 2−5 °C/min were used to identify an approximate value for T_{ODT}. T_{ODT} was then more accurately determined by heating at 0.5 °C/min from a few degrees below the ODT in subsequent measurements (not shown). These values of T_{ODT} are reported in Table 1 and identified by arrows in Figure 3a; an apparent increase of <2 °C in the measured value for T_{ODT} results from the faster heating rates.

This information can be used to estimate $\chi(T)$ for the PS−PVP system. The value of the segregation product χN at which the ODT occurs, $(\chi N)_{ODT}$, can be calculated from the BLFH prediction:[30]

$$(\chi N)_{ODT} = 10.495 + 41.022\bar{N}^{-1/3} \quad (f = 0.50) \qquad (1)$$

where $\bar{N} = Na^6v^{-2}$, N is the number of statistical segments, a is the statistical segment length, and v is the statistical segment volume. This may be rewritten as the product of experimentally measurable parameters: $\bar{N} = (R_0^2/M_n)^3 M_n \rho^2 N_A^2$, where R_0 is the root-mean-square end-to-end distance of the polymer, M_n is the number-average molecular weight, ρ is the mass density, and N_A is Avogadro's number. In the absence of experimental data, we assume that the appropriate physical properties of PVP are identical with those of (structurally similar) PS.[4,47] After correcting for thermal expansion,[47] χ_{ODT} is determined as a function of T_{ODT} (Figure 4); a linear fit to this data yields

$$\chi(T) = 91.6/T - 0.095 \qquad (2)$$

with T measured in degrees K.

This expression for χ is clearly *not* the "true" interaction parameter for the PS−PVP system. The Flory−Huggins interaction parameter is often measured using homopolymer blends.[48−50] For this system, this would require PS and PVP homopolymers (oligomers) of order 10^3 g/mol for phase separation at experimentally accessible temperatures. Not only does the synthesis of monodisperse chains with about 10 repeat units become experimentally intractable, but the value for χ measured with such oligomers may not be applicable to polymers. In addition, experiments suggest that values for χ measured using homopolymer blends and diblocks are not necessarily the same.[51] Despite these limitations, eq 2 serves as a useful predictive tool for estimating T_{ODT} for a given symmetric PS−PVP diblock copolymer.

Isochronal temperature scans of the most asymmetric samples studied, $f_{PS} = 0.35$ and 0.70, indicate that only a single low-temperature phase forms before the ODT. Isothermal frequency scans of this phase (Figure 5a) produce spectra which resemble in form those previously observed for the HEX phases.[21,27] Electron micrographs of unsheared specimens (Figure 5b) show hexagonal arrays of cylinders coexisting with layered structures; the latter projections correspond to cylinders lying in the plane of the section. This establishes the low-temperature phase as hexagonally packed cylinders. SANS results from shear-aligned samples, shown in Figure 5c, confirm this phase assignment. The intensity plot obtained with the neutron beam parallel to the cylinder axis (*i.e.*, in the $\mathbf{q}_y-\mathbf{q}_z$ scattering plane) displays at least three orders of reflections at q^*, $\sqrt{3}q^*$, and $\sqrt{4}q^*$, where $q^* = 2\pi/d_{10}$. Strong Bragg reflections are also found in the $\mathbf{q}_x-\mathbf{q}_y$ plane at $|\mathbf{q}_y| = q^*$ and $\sqrt{4}q^*$, indicating that the (10) plane of the cylinders is parallel to the shear plane. Weak diffuse reflections found in the $\mathbf{q}_x-\mathbf{q}_z$ plane are consistent with this orientation. Note that the $|\mathbf{q}_z| = \sqrt{3}q^*$ reflection in this plane is relatively weak due to a coincident extinction in the cylindrical form factor.

Samples with compositions between that of the lamellar- and cylinder-forming materials display properties characteristic of "nonclassical" morphologies. Rheological scans of the $f_{PS} = 0.65$ material indicate the presence of only a single ordered microstructure below T_{ODT} (not shown); isothermal frequency data suggest a monocontinuous structure (Figure 6a). TEM from an unsheared specimen appears in Figure 6b. The alternating light and dark bands suggest a layered morphology; the presence of light (PS) channels extending into the dark (PVP) layers demonstrate that this morphology is *not* lamellar. The absence of coexisting inverted structures—that is, dark channels extending into light layers—suggests a monocontinuous morphology. SANS examination of presheared specimens, shown in Figure 6c, reveals strong equatorial reflections at q^* with weaker higher order reflections at $2q^*$ in both the $\mathbf{q}_x-\mathbf{q}_y$ and $\mathbf{q}_y-\mathbf{q}_z$ planes. This is consistent with a layered

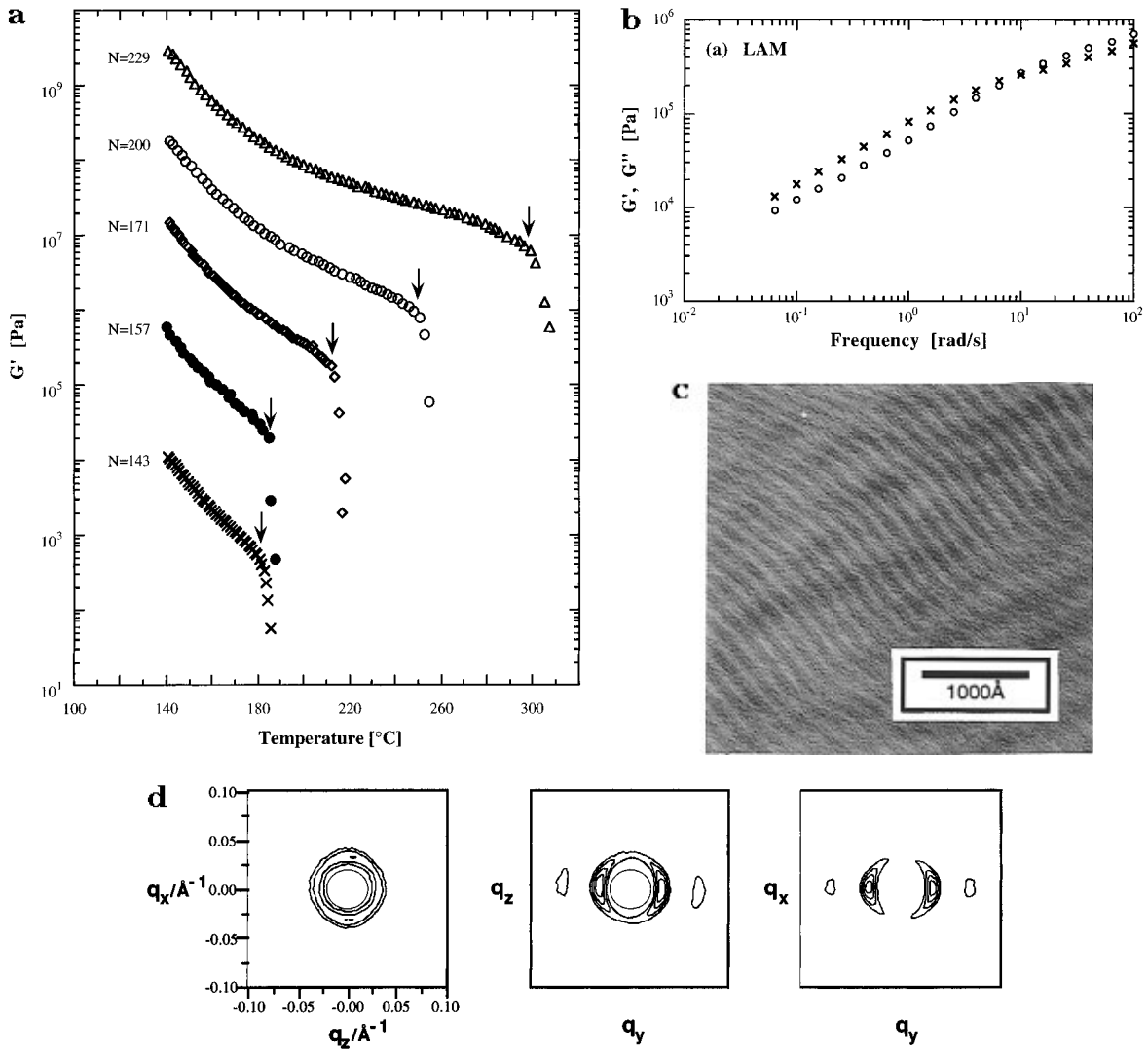

Figure 3. (a) Temperature dependence of the dynamic elastic modulus, G', for a series of symmetric ($f_{PS} = 0.5$) PS−PVP diblock copolymers with varying degrees of polymerization, N. Measurements were made at frequency $\omega = 0.5$ rad/s and 5% strain amplitude while heating at 2−5 °C/min. G' data have been multiplied by the following factors: 10^0 for $N = 143$ (SV-20), 10^2 for $N = 157$ (SV-15), 10^3 for $N = 171$ (SV-17), 10^4 for $N = 200$ (SV-18), 10^5 for $N = 229$ (SV-19). Arrows indicate ODT temperatures from measurements (not shown) where the heating rate was reduced to 0.5 °C/min. (b) Isothermal frequency scans from a nearly symmetric PS−PVP diblock ($f_{PS} = 0.40$) at 140 °C. Dynamic elastic (G', ○) and loss (G'', ×) moduli were measured using 2% or 5% strain amplitudes. The spectrum displays a shape characteristic of a discontinuous structure. (c) Transmission electron micrograph obtained from the $f_{PS} = 0.40$ PS−PVP diblock. Specimens were disordered by heating above the rheologically determined ODT, quenched in liquid nitrogen, annealed at 140 °C for at least 6 h, and then quenched in liquid nitrogen to freeze in the low-temperature morphology. Samples were then ultramicrotomed and stained with iodine; light and dark regions correspond to PS- and PVP-rich microdomains, respectively. These micrographs are representative of the layered structure observed throughout the samples, indicative of a LAM phase. (d) SANS pattern obtained from the $f_{PS} = 0.40$ diblock after preshearing at 140 °C. Reflections appear at positions of q^* and $2q^*$, consistent with a lamellar microstructure. Contours represent logarithmic intensity variations in decade increments. The data around the beam stop has been masked out.

morphology in which the layer planes orient parallel to the shear plane. However, weaker off-equatorial reflections also appear in these images, confirming that the microstructure is not simply lamellar. Scattering from the $\mathbf{q}_x-\mathbf{q}_z$ plane shows some weak features as well, although the symmetry of these structures is not clear from the presheared samples. On the basis of these results, we tentatively identify this microstructure as HPL.

Isochronal temperature sweeps of the $f_{PS} = 0.38$ material show a sudden increase in the dynamic elastic storage modulus (G') at about 155 °C (Figure 7a). Isothermal frequency scans taken above and below this temperature differ considerably (Figure 7b), suggesting that an order−order transition has occurred. The low-temperature phase displays $G'(\omega)$ and $G''(\omega)$ data characteristic of monocontinuous structures,[21,27] while the high-temperature phase shows values for G' that are nearly independent of ω with a high overall elasticity. This solid-like response is consistent with a cubic morphology.[43,52]

In both the low- and high-temperature phases, G' and G'' are independent of strain until a threshold value is reached. Past this point, the moduli depend linearly on applied strain until an amplitude of 6% is reached at a frequency of 0.5 rad/s (see Figure 1). The transition to a nonlinear response depends on frequency, with the phases becoming nonlinear at smaller strains as frequency is increased. Rheological studies of surfactants reveal similar strain limits (1−5%) for bicontinuous cubic phases.[52] The choice of strain amplitudes (2−5%) and frequency for isochronal temperature scans of this material represents a compromise between having sufficient mechanical response to produce measurable stresses while remaining as close as possible to the linear viscoelastic regime.

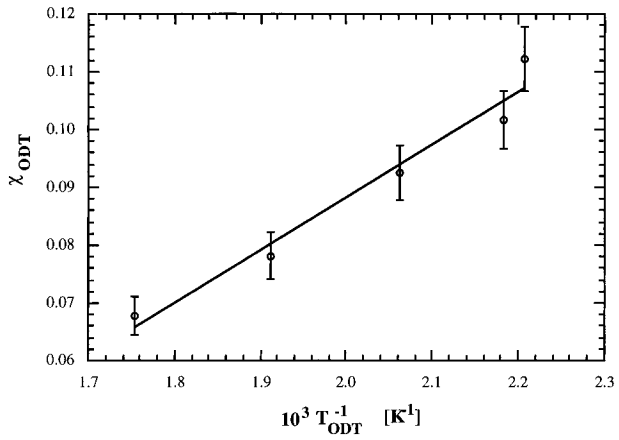

Figure 4. Temperature dependence of the interation parameter, χ, estimated for the PS−PVP system using the rheologically determined order−disorder transition temperature, T_{ODT}, from a series of symmetric ($f_{PS} = 0.50$) diblock copolymers with varying degees of polymerization. The values of χ assume a number of statistical segments per diblock equal to the degree of polymerization and the BLFH theory prediction for $(\chi N)_{ODT}$ given in eq 1. The equation for the line drawn is $\chi(T) = 91.6/T - 0.095$, with T measured in K. Error bars of 5% on the data mainly reflect the uncertainty in the degrees of polymerization calculated from the synthesis stoichiometry.

TEM of the shear-oriented low-temperature phase (Figure 7c) displays alternating light and dark bands with perforations of the light (PS) layers; examination of these perforations along axes nearly perpendicular to the layer planes reveals dark (PVP) spots arranged in a light (PS) matrix. SANS results from a presheared specimen appear in Figure 7d. In the $\mathbf{q}_x-\mathbf{q}_z$ plane, the lowest order reflection consists of six peaks separated by 60°, confirming a hexagonal symmetry in this structure; data in the $\mathbf{q}_y-\mathbf{q}_z$ and $\mathbf{q}_x-\mathbf{q}_y$ planes show an oriented layered structure possessing off-equatorial reflections at angles of about 55° with respect to the position of the layer reflections. In combination with the TEM results, this identifies this structure as HPL, a phase which has been previously identified in several model polyolefin diblock copolymer systems.[19,20]

Layered microstructures have been shown to orient in two distinct ways when subjected to shearing deformation.[19,20,44] The "parallel" orientation places the layer normal along the shear gradient, whereas the "perpendicular" form places the normal along the neutral axis. The scattering pattern in Figure 7d is therefore consistent with scattering from the parallel orientation of the HPL microstructure. Disordering the sample by heating above the ODT, followed by faster shearing at 140 °C, results in a different SANS pattern; see Figure 7e. In the $\mathbf{q}_x-\mathbf{q}_z$ plane, reflections at q^* and $2q^*$ appear along the neutral (x) axis. Four weaker peaks are present at *ca.* ±35° relative to the shear axis at a slightly shorter wavevector, $q' = 0.95q^*$. This scenario is consistent with the perpendicular orientation of the

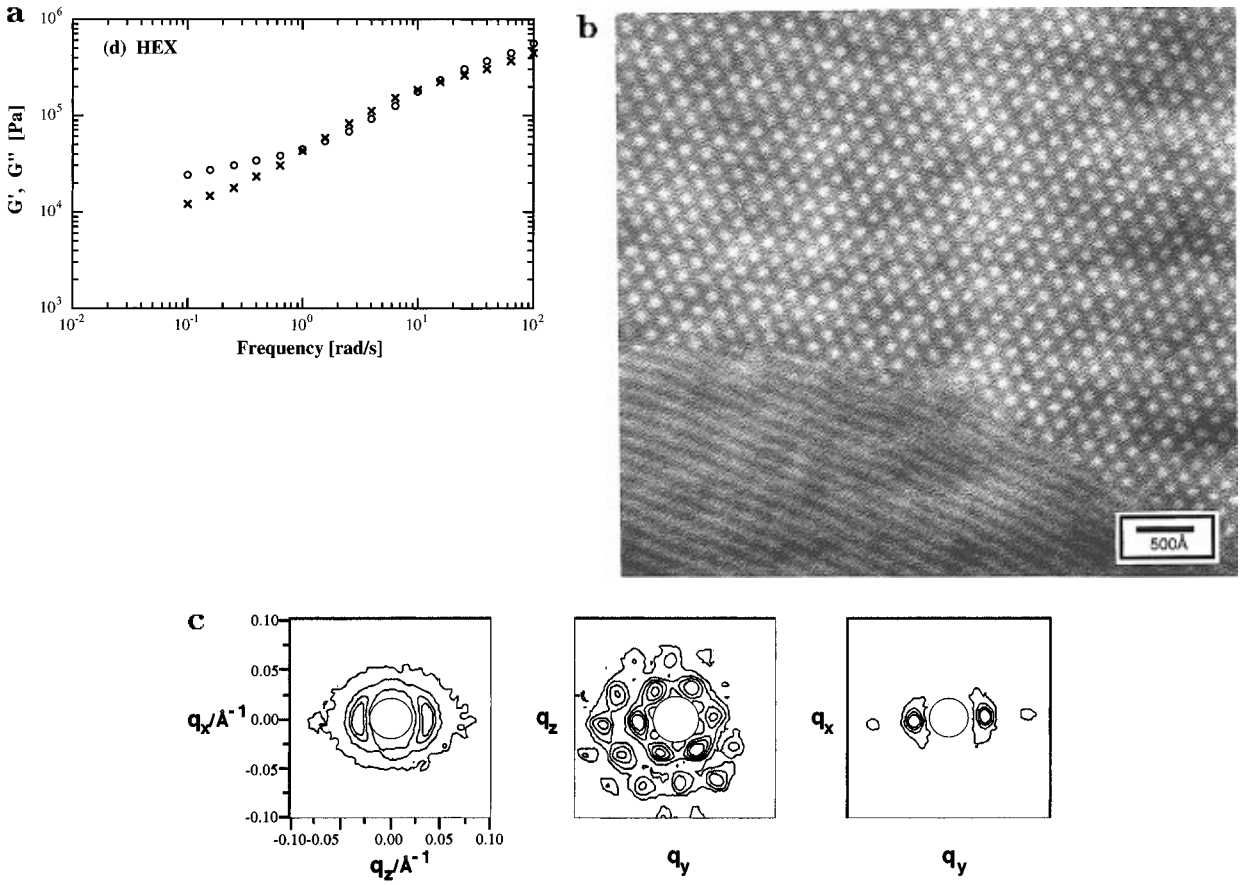

Figure 5. (a) Isothermal frequency scan of the $f_{PS} = 0.35$ diblock at 140 °C. The spectrum resembles that previously observed for monocontinuous morphologies such as HEX. (b) Transmission electron micrograph for the $f_{PS} = 0.35$ specimen after disordering, quenching in liquid nitrogen, annealing at 140 °C for more than 6 h, and then a final quench in liquid nitrogen. Light and dark regions correspond to PS- and PVP-rich microdomains, respectively. These micrographs indicate a HEX morphology, where the spots in a hexagonal array correspond to an end-on view of the cylinders and the layered structures correspond to a side view normal to the cylinder axis. Essentially similar images (with reversed contrast) were recorded from the $f_{PS} = 0.70$ material. (c) SANS patterns recorded from a presheared specimen of the $f_{PS} = 0.35$ material. Peak positions indicate a hexagonal array, consistent with the HEX microstructure. Contours represent logarithmic intensity variations in decade increments. Again, essentially similar diffraction was recorded from the $f_{PS} = 0.70$ material.

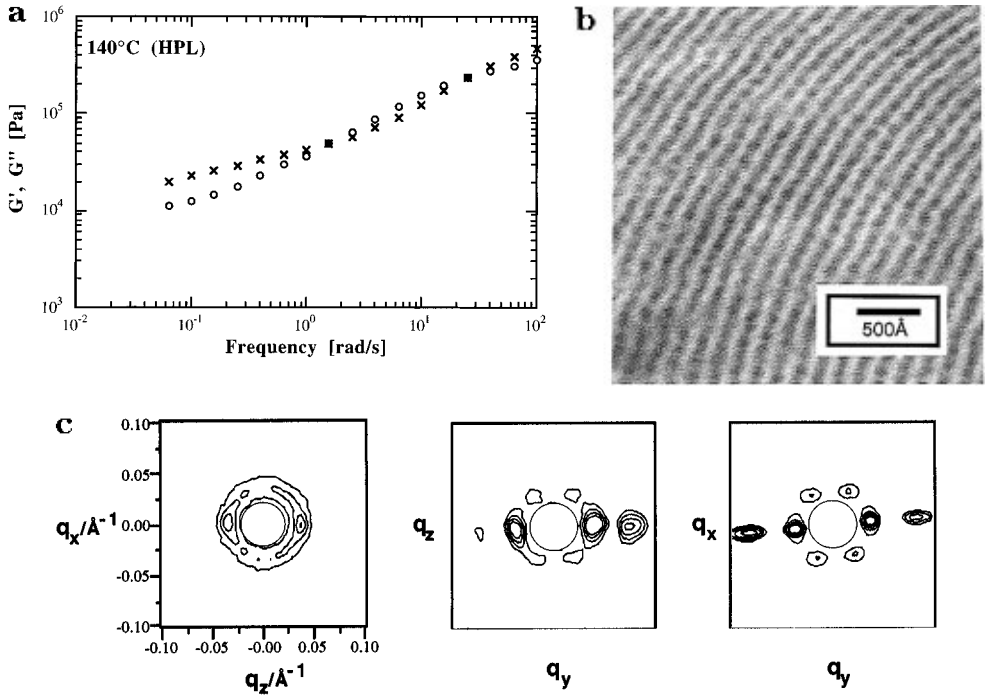

Figure 6. (a) Isothermal frequency scan of the $f_{PS} = 0.65$ diblock at 140 °C. The spectrum resembles that previously observed for a layered structure; compare with the lamellar spectrum in Figure 3b. (b) Transmission electron micrograph from the $f_{PS} = 0.65$ diblock after disordering, quenching, and annealing at 140 °C for 18 h. Light and dark regions correspond to PS- and PVP-rich microdomains, respectively. The morphology appears to be some form of perforated layer structure; the symmetry of the perforations is undetermined. (c) SANS from a presheared specimen of the $f_{PS} = 0.65$ material. The image is consistent with a HPL microstructure. Contours represent logarithmic intensity in decade increments.

HPL microstructure that has been described elsewhere.[19,20]

Heating the sample to 175 °C causes dramatic changes in the observed scattering. SAXS data taken at this point appear in Figure 8a. Two reflections are present at reciprocal space position ratios of $\sqrt{3}:\sqrt{4}$. The spacing and intensity ratios are consistent with previous results for the G/$Ia\bar{3}d$ morphology.[10,21−23,26,27] A TEM micrograph of this state, shown in Figure 8b, reveals an image associated with 3- and 4-fold projections of a bicontinuous cubic unit cell.

The transformation from HPL to G/$Ia\bar{3}d$ can be examined in the shear-aligned material. Upon heating the (initially shear-oriented) $f_{PS} = 0.38$ sample to 175°C without shearing, the scattering pattern from the perpendicular orientation of the shear-oriented HPL phase (Figure 7c) transforms to that shown in scattering pattern c of Figure 7e. The features of these patterns are more clearly discriminated in the corresponding one-dimensional azimuthal intensity plots shown in Figure 8d. This pattern reveals a nearly isotropic ring with a high overall intensity, with some barely discernible reflections superimposed. This suggests that there may be a slightly preferred orientation of the G/$Ia\bar{3}d$ phase when grown from the HPL phase. Epitaxial growth of the G/$Ia\bar{3}d$ bicontinuous phase from the (perpendicular) HPL phase has been reported previously[21] to produce 10 relatively strong reflections, two at ±90°, four at ±19.5°, and four at ±61.7° relative to the shear direction. The associated positions are indicated with arrows. To the extent that individual peaks can be discerned in the azimuthal data shown in Figure 8c, the observed reflection positions agree with those anticipated for the G/$Ia\bar{3}d$ phase. However, the degree of orientation of the bicontinuous structure, qualitatively measured by the azimuthal variation in the scattered intensity, is much lower than that reported previously.[22]

The dynamics of order−order phase transitions can be explored using rheological measurements; of course, results obtained from such measurements are not necessarily applicable to unsheared materials due to symmetry-breaking effects associated with the presence of the shear field. At 140 °C, the frequency response of the $f_{PS} = 0.38$ sample remains stable after 2 h of annealing, suggesting (but not proving) that the HPL phase is in equilibrium; alternatively, the HPL state might be a nonequilibrium structure which is frozen in on this time scale due to the proximity of the glass transition. Upon heating to 152 °C, the specimen transforms to the G/$Ia\bar{3}d$ phase as evidenced by the aforementioned changes in the frequency response. Upon cooling to 140 °C, however, the transition from G/$Ia\bar{3}d$ to HPL does not take place. Frequency sweeps in the cooled state resembled those of the G/$Ia\bar{3}d$ phase except for a shift in ω due to the decreased temperature. Applying a large-amplitude (100%) shear field at 0.1 rad/s recovers a viscoelastic response relatively similar to that of the HPL phase. Upon reheating, the HPL → G/$Ia\bar{3}d$ phase transition is again observed rheologically. Similar behavior in supercooling the G/$Ia\bar{3}d$ bicontinuous phase has been reported in other diblock copolymer systems.[21,27]

From the data, we are unable to determine if the HPL morphology observed in this material is an equilibrium morphology which forms at moderate degrees of segregation or is instead a nonequilibrium structure induced by the shear field. After heating into the disordered state, quenching in liquid nitrogen followed by quiescent annealing at 140 °C produces a poorly ordered, microphase-separated state. No long-range ordering is observed, and we are unable to identify the morphology shown in the micrographs. (Note that the identical procedure in the case of the $f_{PS} = 0.65$ material produced micrographs showing a layered structure reminiscent of HPL.) As the temperature below which the HPL

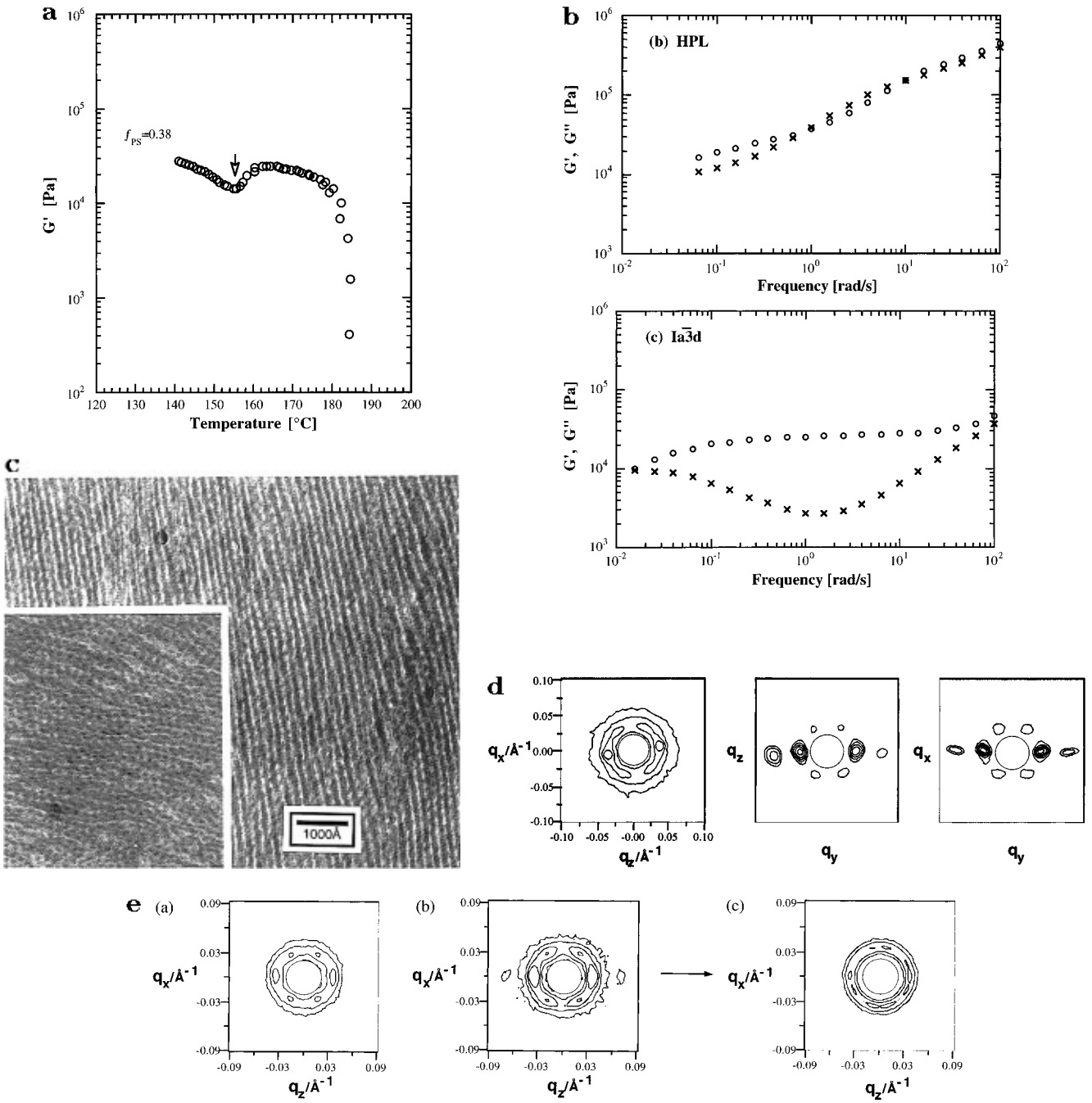

Figure 7. (a) Isochronal temperature scan of the $f_{PS} = 0.38$ material at $\omega = 0.5$ rad/s while heating at about 1 °C/min. The steep decline in G' at the highest temperatures indicates the ODT. The relatively sharp rise in G' indicated by the open arrow is interpreted as signifying an OOT. (b) Dynamic elastic (G', ○) and loss (G'', ×) moduli as a function of frequency at 2% strain amplitude for the $f_{PS} = 0.38$ diblock at 140 and 160 °C, *i.e.*, below and above the suspected OOT identified from the data in Figure 7a. The low-temperature spectrum resembles that observed for the $f_{PS} = 0.65$ material (see Figure 6a); the high-temperature structure displays a spectrum similar to that previously observed for bicontinuous cubic phase structures. (c) TEM from the low-temperature phase of the $f_{PS} = 0.38$ material. To facilitate identification of the structure, the sample was shear-aligned at 140 °C prior to quenching in liquid nitrogen. Light and dark regions correspond to PS- and PVP-rich microdomains, respectively. A layered microstructure with regularly spaced perforations through the minority component (PS) domains is evident. (d) SANS obtained from the (presheared) low-temperature phase of the $f_{PS} = 0.38$ material. Contours depict logarithmic intensity variations in decade increments. The images are consistent with a HPL morphology, in accordance with TEM results (Figure 7c). (e) SANS data for the $f_{PS} = 0.38$ diblock obtained with the *in situ* shearing device at 300% strain amplitude. The left-hand image shows data obtained after application of a shear rate of 0.19 s^{-1} at 140 °C, corresponding to HPL in the parallel orientation, while the right-hand image presents data obtained from a different specimen at a rate of 0.95 s^{-1} at 140 °C, showing the HPL phase in the perpendicular orientation. The azimuthal intensity plots prepared from these images were generated by integrating counts as a function of azimuthal angle in a radial band extending from $0.8q^*$ to $1.2q^*$, where q^* is the location of the lowest order scattering maximum. The curve corresponding to the parallel orientation shows six weak reflections separated by 60°, as expected; the curve generated from the perpendicular data shows strong equatorial reflections with weaker reflections at ±35° to the equatorial axis, also as expected.

phase might be in equilibrium (140 °C) is relatively close to the glass transition temperatures of the blocks (100 °C), any kinetics associated with the development of long-range order are expected to be extremely slow, and so the absence of such order is not surprising. Furthermore, if the HPL is an equilibrium structure, such effects would also interfere with the observation of a G/$Ia\bar{3}d$-to-HPL transition upon cooling. Given these

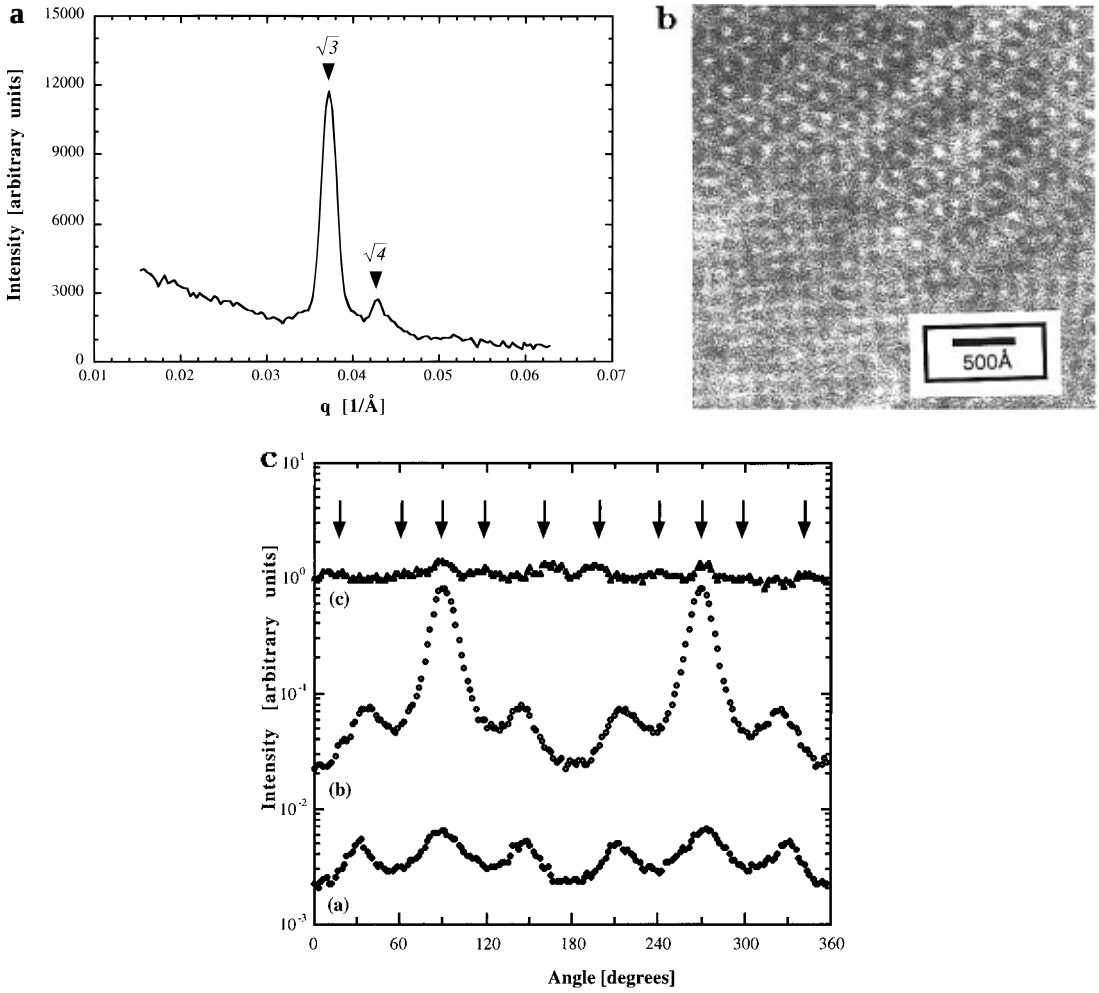

Figure 8. (a) Small-angle X-ray scattering powder pattern obtained from the high-temperature ordered phase in the $f_{PS} = 0.38$ PS−PVP sample. The first two reflections have a q-spacing ratio of $\sqrt{3}:\sqrt{4}$, consistent with the $Ia\bar{3}d$ space group. (b) Transmission electron micrograph obtained from the $f_{PS} = 0.38$ PS−PVP sample after disordering, quenching in liquid nitrogen, annealing for 6 h at 170 °C, and quenching in liquid nitrogen prior to ultramicrotoming and staining with iodine. Light and dark regions correspond to PS- and PVP-rich microdomains, respectively. An interconnected morphology with both 3-fold (upper region of image) and 4-fold (lower region) projections can be discerned, indicative of a bicontinuous cubic structure. (c) One-dimensional azimuthal integrations of SANS data for the $f_{PS} = 0.38$ diblock obtained with the *in situ* shearing device at 300% strain amplitude, prepared by plotting the integrated intensity in a band of ±20% about the principal wavevector q^* as a function of azimuthal angle. The lowest image, a, shows the low-temperature HPL phase in the perpendicular orientation with the beam parallel to the layer normals; the presence of six reflections at 60° intervals establishes a hexagonal packing for the perforations. The data in profile b was recorded with the beam in the plane of the layers; the two strong reflections separated by 180° arise from the orientation of the perforated lamellae, while the four weaker reflections on either side of these reflections are due to the packing of the perforations. Heating this material to 175 °C in the absence of shear results in profile c. Arrows indicate anticipated reflection positions from the G/$Ia\bar{3}d$ microstructure when grown epitaxially from the perpendicular orientation of HPL. The relatively flat shape of the high-temperature curve implies that the G/$Ia\bar{3}d$ phase grows with only a slightly preferred orientation from the HPL microstructure in this sample.

limitations, we report an OOT temperature for this material using the average of the rheologically determined transition temperatures upon heating (152 °C) and cooling (140 °C), and we note that the phase behavior observed in this sample may change in the absence of a shear field.

Discussion

Figure 9 summarizes our results in the form of a χN versus f_{PS} "phase diagram", along with illustrations of the observed microstructures. (Here we note that this depiction is not a proper thermodynamic representation because f_{PS} is not a true intensive variable, that is, the composition f_{PS} cannot be varied continuously in these one-component systems. Nevertheless, this is the most convenient way to convey the results.) Values of χN are estimated using the $\chi(T)$ from eq 2 with the OOT and ODT temperatures of each sample. OOT and ODT temperatures are indicated by open and solid symbols, respectively, and the crosses identify the experimental limit in χN dictated by the PS−PVP glass transition. The order−disorder phase boundary has been drawn in this diagram by following the apparent trends in the $(\chi N)_{ODT}$ values. Vertical lines show the range of χN explored for each sample, and the phases indicated have been identified in the previous section. This work does not eliminate the possibility of finding additional phases at intermediate values of composition or at higher values of χN. Establishing the detailed phase behavior of PS−PVP diblock copolymers is hindered by the necessity to synthesize a new sample at each target composition. In a subsequent report,[53] we will present a more detailed "phase diagram" by exploring the regions where complex phase behavior is expected (*i.e.*, between the LAM and HEX phases)[2,18−21,27] using PS−PVP diblock blends.

We are unaware of any previous publications identifying the combination of PS−PVP diblock copolymer

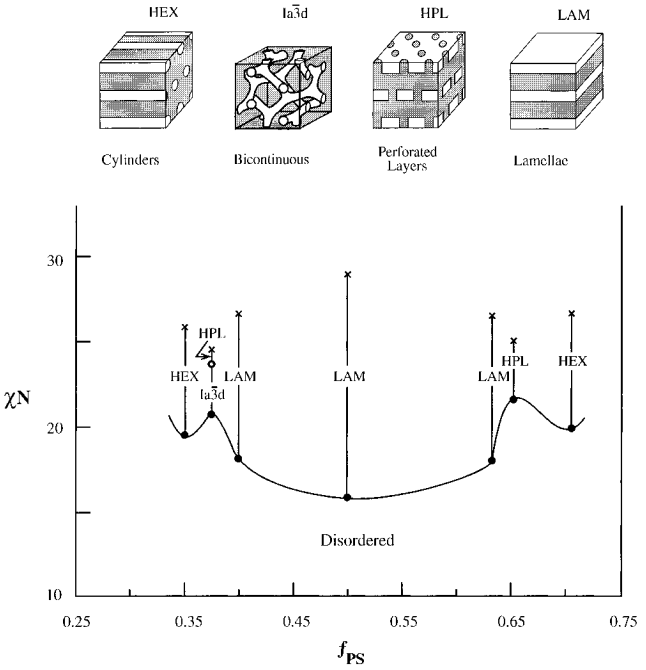

Figure 9. Summary of results found for the pure PS−PVP diblock copolymer samples reported in this work. Values of χN are estimated using $\chi_{PS-PVP} = 91.6/T - 0.095$ with the rheologically determined OOT and ODT temperatures of each sample. Symbols are as follows: (○) OOT, (●) ODT, (×) experimental limit in χN dictated by the PS−PVP glass transition. Phase notation is as follows: LAM, lamellae; HPL, hexagonally perforated layers; *Ia*$\bar{3}$*d*, bicontinuous network formed by planar tripod connectors with indicated space group symmetry (also referred to as the gyroid* structure); HEX, hexagonally packed cylinders. The order−disorder phase boundary has been drawn in this diagram by following the apparent trends in the $(\chi N)_{ODT}$ values. Vertical lines show the range of χN explored *via* rheological methods for each sample.

phases reported in Figure 9. Recently, the HPL[21,26] and bicontinuous G/*Ia*$\bar{3}$*d*[21,23,26] phases have also been discovered near the ODT in the PI−PS system. In both systems, these phases exist over a relatively narrow range in composition between the LAM and HEX phases. Although only the HPL phase has been identified between the LAM and HEX phases for $f_{PS} > 0.5$ in the (pure) PS−PVP diblock copolymers described here, experiments using diblock copolymer blends suggest that the G/*Ia*$\bar{3}$*d* phase is stable in this region as well.[53] A nearly symmetric phase diagram for the PS−PVP system is anticipated due to the structural similarity between the two repeat units, although the statistical segment lengths of the PS and PVP may differ somewhat causing slight asymmetry. An important conclusion from this work is that the occurrence of complex phases (*i.e.*, HPL and G/*Ia*$\bar{3}$*d*) are bound in composition between the LAM and HEX phases at $0.35 < f_{PS} < 0.40$ and $0.63 < f_{PS} < 0.70$ in the PS−PVP system.

An OOT has been identified between the HPL and G/*Ia*$\bar{3}$*d* phases. To the best of our knowledge, order−order phase transitions have not previously been reported in PS−PVP diblock copolymer melts, although in an earlier report we have identified an OOT between the HEX and G/*Ia*$\bar{3}$*d* phases in a PS−PVP diblock blend.[22] The disordered phase is accessible directly from both the HPL and G/*Ia*$\bar{3}$*d* bicontinuous phases in the PS−PVP system. The HPL phase extends from the ODT beyond the limits accessible in this experiment, while the G/*Ia*$\bar{3}$*d* phase is confined to a region near the ODT in the sample reported here. We will demonstrate elsewhere,[53] using diblock copolymer blends, that the localization of the bicontinuous G/*Ia*$\bar{3}$*d* phase near the ODT is a general feature of the PS−PVP phase diagram.

The HPL phase occurs in a wide range of block copolymer systems.[19−21,26] Note, however, that HPL signifies in-plane hexagonal perforation symmetry but does not imply a particular layer-by-layer stacking sequence (results show that adjacent perforated layers are staggered, still leaving many possible sequences, *i.e.*, *abab*..., *abcabc*..., random, etc.). The differences in free energy between the various (staggered) stacking sequences are likely to be very small. A complete discussion of the stacking in the hexagonal layered phases lies outside the scope of this paper. However, we recognize that the off-equatorial SANS reflections from the perpendicular orientation of the HPL phase in the PI−PS system[21] are evident at ±19.5° from the shear direction, while those in the PS−PVP system are located at ±34° from the shear direction (see Figure 8c). This implies that the stacking sequences of the perforations may differ between the PI−PS and PS−PVP systems. The stacking in the PI−PS system was speculated to be consistent with the *abcabc*... sequence,[21] although the particular stacking sequences present cannot be definitively identified in either case. However, we hypothesize that the stacking sequence in the HPL phase may have consequences on the epitaxial growth of the bicontinuous G/*Ia*$\bar{3}$*d* phase. An epitaxial relationship between the HPL and G/*Ia*$\bar{3}$*d* phases has been reported previously for a PI−PS diblock copolymer.[21] The proposed *abcabc*... stacking sequence offered a possible geometric relationship that matched the angle between the layers and the perforations in the HPL phase with the angles of the {211} planes and [111] direction in the G/*Ia*$\bar{3}$*d* phase. This suggested the epitaxial relationship (001) ↔ ($\bar{2}$11) between the HPL and G/*Ia*$\bar{3}$*d* phases with the [$\bar{1}$11] direction of the G/*Ia*$\bar{3}$*d* phase along one set of lines connecting the centers of the perforations in the HPL structure. The epitaxy from the HPL phase to the G/*Ia*$\bar{3}$*d* in the PI−PS system[21] produced 10 strong reflections, two at ±90°, four at ±19.5°, and four at ±61.7° relative to the shear direction. In contrast, the transition from HPL to G/*Ia*$\bar{3}$*d* in the PS−PVP system results in a nearly isotropic high-intensity scattering pattern. This indicates that the G/*Ia*$\bar{3}$*d* phase grows in all orientations from the HPL phase, although there is a slight preferential orientation with the [111] direction along the shear direction as in PI−PS.[21] The difference in the mechanism of growth in this phase transition could be related to a different stacking sequence of the layers in the HPL phase. The three-dimensional epitaxy from a layered structure to the G/*Ia*$\bar{3}$*d* phase may involve a complex mechanism that incorporates the particular stacking sequence of the layers in the HPL phase. Further investigation of these phases and phase transitions may provide insight into this interesting result.

Summary

The complex phase behavior of PS−PVP diblock copolymer melts near the ODT has been investigated using a variety of well-established experimental techniques including DMS, TEM, SANS, and SAXS. Determining the phase behavior of the block copolymers relied on information from each of the characterization techniques employed in this study. Rheology was used to identify order−order and order−disorder phase transition temperatures. Accurate assignment of a microstructure to the various phases depended on TEM, SANS, and SAXS analyses. TEM provided real-space morphology images which established certain features

associated with the microstructures, whereas SANS and SAXS analyses were used to identify the symmetry of the microstructures.

The temperature dependence of the PS−PVP interaction parameter has been estimated as $\chi(T) = 91.6/T - 0.095$, using the predictions of the BLFH theory for the ODT temperatures of a series of symmetric ($f_{PS} = 0.50$) diblocks. Because PS−PVP diblocks possess a relatively large χ parameter, placing the order−disorder transition at experimentally tractable temperatures requires relatively low molecular weights (≈20 000 g/mol). Four ordered microstructures have been identified in the composition range $0.35 \lesssim f_{PS} \lesssim 0.70$ in the PS−PVP diblock copolymer system. HEX exist at PS volume fractions $f_{PS} = 0.35$ and 0.70, and LAM are present at $f_{PS} = 0.40$ and 0.63. More complex microstructures have been identified between these two phases on both sides of the phase diagram. A HPL phase exists at $f_{PS} = 0.38$ and 0.65. An order−order transition between the HPL phase and the bicontinuous cubic G/$Ia\bar{3}d$ phase occurs at $f_{PS} = 0.38$. The latter phase is confined to a region near the ODT, while the former extends further from the ODT beyond the limits accessible in these experiments. Approximate composition boundaries for the existence of complex phases (*i.e.*, HPL and G/$Ia\bar{3}d$) are established between $0.35 < f_{PS} < 0.40$ and $0.63 < f_{PS} < 0.70$, where the LAM and HEX phases occur at these limits in the PS−PVP system.

The particular stacking sequence could not be identified in the HPL microstructure. However, it is noted that, in contrast to other block copolymer systems, the G/$Ia\bar{3}d$ phase does not seem to grow with a preferred orientation from the HPL phase in the PS−PVP system. This suggests that the layer-stacking sequence influences the epitaxial relationship between these two microstructures.

Acknowledgment. Support for this research was provided by the U.S. Air Force Office of Scientific Research (AF/F49620-93-1-0182) and the Center for Interfacial Engineering (CIE), an NSF-sponsored engineering research center at the University of Minnesota. Work at Princeton University was supported by the National Science Foundation (DMR-922-3966) and the U.S. Department of Energy (DE-FG02-87ER60522).

References and Notes

(1) Hasegawa, H.; Tanaka, H.; Yamasaki, K.; Hashimoto, T. *Macromolecules* **1987**, *20*, 1651.
(2) Bates, F. S.; Schulz, M. F.; Khandpur, A. K.; Förster, S.; Rosedale, J. H.; Almdal, K.; Mortensen, K. *J. Chem. Soc., Faraday Trans.* **1994**, *98*, 7.
(3) Vavasour, J. D.; Whitmore, M. D. *Macromolecules* **1993**, *26*, 7070. Matsen, M. W.; Schick, M. *Macromolecules* **1994**, *27*, 4014.
(4) Fetters, L. J.; Lohse, D. J.; Richter, D.; Witten, T. A.; Zirkel, A. *Macromolecules* **1994**, *27*, 4639.
(5) *Block Polymers*; Aggarwal, S. L., Ed.; Plenum Press: New York, 1970.
(6) *Colloidal and Morphological Behavior of Block and Graft Copolymers*; Molau, G. E., Ed.; Plenum Press: New York, 1971.
(7) Gallot, B. R. M. *Adv. Polym. Sci.* **1978**, *29*, 85.
(8) Schulz, M. F.; Bates, F. S. In *AIP Handbook of Polymer Properties*; Mark, J., Ed.; in press.
(9) Thomas, E. L.; Alward, D. B.; Kinning, D. J.; Handlin, D. L.; Fetters, L. J. *Macromolecules* **1986**, *19*, 2197.
(10) Hajduk, D. A.; Harper, P. E.; Gruner, S. M.; Honeker, C. C.; Thomas, E. L.; Fetters, L. J. *Macromolecules* **1995**, *28*, 2570.
(11) Helfand, E.; Wasserman, Z. R. In *Developments in Block Copolymers*; Goodman, I., Ed.; Applied Science: London, 1982; Vol. 1, p 99.
(12) Semenov, A. N. *Sov. Phys. JETP* **1985**, *61*, 733.
(13) Likhtman, A. E.; Semenov, A. N. *Macromolecules* **1994**, *27*, 3103.
(14) Olmsted, P. D.; Milner, S. T. *Phys. Rev. Lett.* **1994**, *72*, 936; **1995**, *74*, 829.
(15) Matsen, M. W.; Schick, M. *Phys. Rev. Lett.* **1994**, *72*, 2660.
(16) Hamley, I. W.; Bates, F. S. *J. Chem. Phys.* **1994**, *100*, 6813.
(17) Anderson, D. M.; Thomas, E. L. *Macromolecules* **1988**, *21*, 3221.
(18) Almdal, K.; Koppi, K. A.; Bates, F. S.; Mortenson, K. *Macromolecules* **1992**, *25*, 1743.
(19) Hamley, I. W.; Koppi, K. A.; Rosedale, J. H.; Bates, F. S.; Almdal, K.; Mortensen, K. *Macromolecules* **1993**, *26*, 5959.
(20) Hamley, I. W.; Gehlsen, M. D.; Khandpur, A. K.; Koppi, K. A.; Rosedale, J. H.; Schulz, M. F.; Bates, F. S.; Almdal, K.; Mortensen, K. *J. Phys. II (France)* **1994**, *4*, 2161.
(21) Förster, S.; Khandpur, A. K.; Zhao, J.; Bates, F. S.; Hamley, I. W.; Ryan, A. J.; Bras, W. *Macromolecules* **1994**, *27*, 6922.
(22) Schulz, M. F.; Bates, F. S.; Almdal, K.; Mortensen, K. *Phys. Rev. Lett.* **1994**, *73*, 86.
(23) Hajduk, D. A.; Harper, P. E.; Gruner, S. M.; Honeker, C. C.; Kim, G.; Thomas, E. L.; Fetters, L. J. *Macromolecules* **1994**, *27*, 4063.
(24) Hajduk, D. A.; Gruner, S. M.; Rangarajan, P.; Register, R. A.; Fetters, L. J.; Honeker, C.; Albalak, R. J.; Thomas, E. L. *Macromolecules* **1994**, *27*, 490.
(25) Sakurai, S.; Kawade, H.; Hashimoto, T.; Fetters, L. J. *Macromolecules* **1993**, *26*, 5796.
(26) Khandpur, A. K.; Förster, S.; Bates, F. S.; Hamley, I. W.; Ryan, A. J.; Bras, W. *Macromolecules* **1995**, *28*, 8796.
(27) Zhao, J.; Majumdar, B.; Schulz, M. F.; Bates, F. S.; Almdal, K.; Mortensen, K.; Hajduk, D. A.; Gruner, S. M. *Macromolecules* **1996**, *29*, 1204.
(28) Bates, F. S.; Fredrickson, G. H. *Annu. Rev. Phys. Chem.* **1990**, *41*, 525.
(29) Leibler, L. *Macromolecules* **1980**, *13*, 1602.
(30) Fredrickson, G. H.; Helfand, E. *J. Chem. Phys.* **1987**, *87*, 697.
(31) Barrat, J.-L.; Fredrickson, G. H. *J. Chem. Phys.* **1991**, *95*, 1281.
(32) Fredrickson, G. H. *Macromolecules* **1991**, *24*, 3456.
(33) Brazovskii, S. A. *Sov. Phys. JETP* **1975**, *41*, 88.
(34) Brazovskii, S. A.; Dzyaloshinskii, I. E.; Moratov, A. R. *Sov. Phys. JETP* **1987**, *66*, 625.
(35) Muthukumar, M. *Macromolecules* **1993**, *26*, 5259.
(36) Almdal, K.; Bates, F. S.; Mortensen, K. *J. Chem. Phys.* **1992**, *96*, 9122.
(37) Bates, F. S.; Rosedale, J. H.; Fredrickson, G. H.; Glinka, C. J. *Phys. Rev. Lett.* **1988**, *61*, 2229.
(38) Koppi, K. A.; Tirrell, M.; Bates, F. S. *Phys. Rev. Lett.* **1993**, *70*, 1449.
(39) Rosedale, J. H.; Bates, F. S. *Macromolecules* **1990**, *23*, 2329.
(40) Balsara, N. P.; Lin, C. C.; Dai, H. J.; Krishnamoorti, R. *Macromolecules* **1994**, *27*, 1216.
(41) Gilman, H.; Cartledge, F. K. *J. Organomet. Chem.* **1964**, *2*, 447.
(42) Möller, M.; Lenz, R. W. *Makromol. Chem.* **1989**, *190*, 1153.
(43) Koppi, K. A.; Tirrell, M.; Bates, F. S.; Almdal, K.; Mortensen, K. *J. Rheol.* **1994**, *38*, 999.
(44) Koppi, K. A.; Tirrell, M.; Bates, F. S.; Almdal, K.; Colby, R. H. *J. Phys. II (France)* **1992**, *2*, 1941.
(45) Tate, M. W.; Eikenberry, E. F.; Gruner, S. M. In preparation.
(46) Rosedale, J. H.; Bates, F. S.; Almdal, K.; Mortensen, K.; Wignall, G. D. *Macromolecules* **1995**, *28*, 1429.
(47) *Polymer Handbook*, 2nd ed.; Brandrup, J., Immergut, E. H., Eds.; Wiley: New York, 1975.
(48) Flory, P. J. *J. Chem. Phys.* **1942**, *10*, 51.
(49) Huggins, M. *J. Phys. Chem.* **1942**, *46*, 151.
(50) Huggins, M. *J. Am. Chem. Soc.* **1942**, *64*, 1712.
(51) Bates, F. S.; Maurer, W. W.; Lodge, T. P.; Unpublished results.
(52) Radiman, S.; Toprakcioglu, C.; McLeish, T. *Langmuir* **1994**, *10*, 61.
(53) Schulz, M. F.; Khandpur, A. K.; Matsen, M. W.; Bates, F. S.; Almdal, K.; Mortensen, K.; Hajduk, D. A.; Gruner, S. M. In preparation.

MA951714A